Hydrogenation of levulinic acid into gamma-valerolactone over in situ reduced CuAg bimetallic catalyst: Strategy and mechanism of preventing Cu leaching

Li Zhang[a], Jingbo Mao[a,c], Shenmin Li[a], Jingmei Yin[a], Xudong Sun[a], Xinwen Guo[c], Chunshan Song[b,c,*], Jinxia Zhou[a,b,c,*]

[a] Liaoning Engineering Laboratory of Special Optical Functional Crystals, College of Environmental and Chemical Engineering, Dalian University, Dalian, 116622, China
[b] Clean Fuels & Catalysis Program, EMS Energy Institute, Departments of Energy and Mineral Engineering and of Chemical Engineering, The Pennsylvania State University, 209 Academic Projects Building, University Park, PA 16802, USA
[c] State Key Laboratory for Fine Chemicals, PSU-DUT Joint Center for Energy Research, School of Chemical Engineering, Dalian University of Technology, Dalian 116024, China

ARTICLE INFO

ABSTRACT

Metal leaching is a major issue in efficient production of γ-valerolactone (GVL) from levulinic acid (LA) under mild reaction conditions. In this study, Ag was added to Cu-supported γ-Al$_2$O$_3$ catalyst to suppress Cu leaching in the hydrogenation of LA into GVL. The CuAg/Al$_2$O$_3$ catalyst was reduced in situ during the reaction, and Cu leaching in the solution was significantly suppressed. The bimetallic catalyst without reduction pretreatment achieved approximately 100% yield to GVL and exhibited good reusability in nine consecutive cycles under mild reaction conditions of 180 °C and 1.4 MPa H$_2$ pressure in tetrahydrofuran (THF). The strong interplay in the geometric and electronic effects between Cu and Ag was verified through XPS, H$_2$-TPR, TEM, STEM/EDS, and XRD analyses. This paper extensively discussed the mechanism of Ag on preventing Cu leaching and the superiority of in situ reduction in solution over external reduction in gas.

1. Introduction

The diminishing fossil fuel resources and the increasing concern for serious environmental issues, such as airborne pollution and climate change, have promoted the utilization of biomass resources as renewable feedstock to generate fuels and chemicals [1,2]. As a versatile biochemical, gamma-valerolactone (GVL) is one of the top value-added products from biomass [3,4]. GVL is renewable and stable and can be used as precursor of clean fuel, green solvent in fine chemical synthesis and food additives, or as intermediate in synthesis of value-added chemicals [5,6]. Over the last two decades, researchers have developed a variety of methods for efficient synthesis of GVL from levulinic acid (LA), a bio-platform chemical that can be produced from renewable lignocellulosic biomass, through various domino reaction pathways [3,4]. The two typical approaches for the hydrogenation of LA or its esters to GVL include transfer hydrogenation using formic acid or alcohols as hydrogen donor and direct hydrogenation using molecular hydrogen (H$_2$) as hydrogen donor [3,4]. The former approach has been extensively investigated over a series of metal catalysts or Zr-based materials [7–10], but its application is limited by the high cost of the

hydrogen donors. In contrast, direct hydrogenation using H$_2$ is more advantageous and shows a great potential for commercial application [11].

Homogeneous catalysts offer good activity and high selectivity for hydrogenation of LA to GVL under mild conditions [12]. However, homogeneous catalysts are difficult to recycle and are often not environmentally friendly [3,4]. In this regard, heterogeneous catalysts, including noble metal catalysts and non-noble metal catalysts, have received considerable attention for GVL production [3,4]. In particular, Ru catalysts have been widely investigated [13–16], and other noble metal catalysts, such as Rh, Pd, Pt, and Au catalysts [16–18], have also been tested to synthesize GVL from LA. Several noble metal catalysts exhibit good catalytic activity. At the same time, some researchers have focused on cheap non-noble metal catalysts, such as Ni-based [19–24], Cu-based [25–30] catalysts, for the production of GVL. Ni-based catalysts, such as Ni/Al$_2$O$_3$ [19], Ni-MoO$_x$/C [20], and Ni/boehmite [21], show relatively high selectivity to GVL but poor stability in subsequent catalytic cycles. Gundekar et al. [21] found that the decrease in the successive conversion of LA is due to severe Ni leaching into the solution in each cycle. Cu-Al$_2$O$_3$ and Cu-ZrO$_2$ exhibit 100 mol.% selectivity

to GVL when catalyzing LA hydrogenation at a low temperature of 200 °C; nevertheless, leaching of active metal Cu under mild reaction conditions is a serious issue [25,26]. Severe Cu leaching can be indicated by the blue color of the reaction solvent. This color was due to the formation of a soluble metal carboxylate complex with LA [25]. Metal leaching [3,7,21,25,26] deactivates the supported metal catalysts, contaminates the product, and increases the cost for product purification. Metal leaching could be avoided when the carboxyl group of LA undergoes esterification with alcohols before being in contact with the catalyst [7,25]. However, the esterification route consumes alcohols, thereby complicating the process. In this regard, it is desired to focus on solving issues related to metal leaching during LA hydrogenation under mild reaction conditions. In most cases, Ni- and Cu-based catalysts should undergo external reduction at 300 °C–700 °C in H_2 before placing them in the reaction systems [19,20,22–29]. In principle, the operation and maintenance costs can be substantially decreased by omitting the harsh external reduction. Few studies were conducted to develop in situ reduction methods for preparation of catalysts [21,30]. In situ reduction typically comprises two methods. First, the catalyst is initially reduced in the reactor by reducing gases, such as H_2, and the reaction mixtures are then added in the reactor for the reaction [30]. This method is similar to conventional pre-reduction treatment but does not remove the catalyst from the reactor. Second, the catalyst is reduced and activated during the course of the reaction under the same conditions [21]. Gundekari et al [21] transformed NiAl-layered double hydroxide into Ni/boehmite in situ under the reaction conditions of 200 °C and 4 MPa H_2. The in situ-formed catalyst showed good catalytic activity in the hydrogenation of LA to GVL for the first run but was deactivated during reusage due to Ni leaching. In our previous study on the selective hydrogenolysis of glycerol to propane-diols, we found that the addition of Ag to the Cu/Al_2O_3 catalyst induced the in situ reduction of CuO during the reaction [31]. Despite the good catalytic performance of the CuAg bimetallic catalyst on glycerol hydrogenolysis, systematic studies are lacking regarding the properties of the catalyst, including the structures of the Cu and Ag nanoparticles, the differences in the performances between in situ reduction during the reaction and the external reduction in reducing gas, and the electronic synergy between Cu and Ag.

In this study, Ag was added to Cu-supported γ-Al_2O_3 catalyst to prevent Cu leaching during the hydrogenation of LA into GVL. The in situ reduction of the $CuAg/Al_2O_3$ catalyst promoted by Ag under mild reaction conditions led to approximately 100 mol.% yield to GVL and good stability in consecutive cycles. The characteristic of Cu leaching and the mechanism of Ag in preventing metal leaching from the catalyst were extensively discussed. Moreover, the superiority of the in situ reduction of the catalyst during the reaction was established by comparing with external reduction in reducing gas.

2. Experimental

2.1. Catalyst preparation

The catalysts were prepared by incipient wetness impregnation method [31–33]. Briefly, aqueous solutions of $Cu(NO_3)_2·3H_2O$ and/or $AgNO_3$ were used as precursor, γ-Al_2O_3 (Shandong Filiale of China Aluminum Co., Ltd., calcined at 550 °C in air before use). The impregnation mixtures were dried at 110 °C for 12 h and then underwent calcinations at 450 °C in air for 3 h. Unless stated otherwise, these catalysts after the calcinations were used in reactions directly. The catalysts prepared were designated as Cu_xAg_y/Al_2O_3, in which x and y represent the amount of Cu and Ag metals loaded on per gram γ-Al_2O_3 (mmol/g), respectively. For example, $Cu_{0.8}Ag_{0.8}/Al_2O_3$ is a catalyst with 0.8 mmol Cu and 0.8 mmol Ag loaded on 1 g of γ-Al_2O_3. For comparative analysis, a few Cu_x/Al_2O_3 sample was reduced at 350 °C for 2 h in a 5 vol.% H_2/Ar stream (30 ml/min), and the reduced sample was named as Cu_x/Al_2O_3-H_2. The catalysts were in powder forms and

the particle sizes were within 0.13 mm in diameters. CuO powder and metal Cu powder were prepared for metal leaching tests. $Cu(OH)_2$ was precipitated using $Cu(NO_3)_2·3H_2O$ as precursor and NaOH as precipitant and calcined to obtain CuO. Metal Cu powder was acquired through the reduction of CuO at 350 °C for 2 h in 5 vol.% H_2/Ar stream (30 mL/min).

2.2. Catalyst characterization

Surface species of the catalysts were characterized by X-ray photoelectron spectroscopy (XPS) analyzer [ESCALAB-250, Al Kα monochromatic X-ray source (E = 1486.6 eV), and 50 eV pass energy]. The adventitious C 1s peak (284.6 eV) was used as reference to align the spectra, and XPSPEAK 41 program was used for mathematical analysis of the peaks in the spectra. The reduced properties of the metal oxides on the catalysts were analyzed by self-assembly temperature-programmed reduction (TPR). For each test, 50 mg of the sample was dried in argon and reduced in 5 vol.% H_2/Ar gas mixture (30 mL/min) at a linear heating rate of 10 °C/min. Hydrogen consumption was monitored by TCD detector. Micromeritics ASAP 2020 gas adsorption apparatus (USA) was used to measure Brunauer–Emmett–Teller specific surface area (S_{BET}) and pore volume. The metal content in the solution was determined by an inductively coupled plasma-optical emission spectroscopy instrument (ICP-OES, Optima7000DV, Perkin Elmer Ltd.). X-ray diffraction (XRD) analysis of the catalysts was performed on an X-ray diffractometer (M/s. Rigaku Corporation, Japan) at 30 kV and 15 mA with Ni-filtered Cu-Kα radiation. Thermogravimetric analysis (TGA) was performed on a TGA/SDTA851e instrument (Mettler Toledo) from room temperature to 700 °C (10 °C/min) in a flow of air gas (20 mL/min). The morphology of the catalysts was characterized by transmission electron microscopy (TEM, Tecnai F30 system at 300 kV) and high-resolution TEM (HRTEM) analyses. Scanning transmission electron microscopy combined with energy-dispersive X-ray spectroscopy (STEM/EDS) was conducted on the same microscope to acquire the elemental map of the spent catalyst on carbon-coated molybdenum grid. The product structures were analyzed by gas chromatography–mass spectrometry (Agilent 6890N-5973N GC–MS).

2.3. Catalytic performance measurement

LA hydrogenation was carried out in a batch reactor system consisting of a stainless steel autoclave (25 mL) under magnetic stirring (Beijing Century Senlong Experimental Apparatus Co., Ltd.). In a typical run, 300 mg of LA, 150 mg of dry catalyst and 6 mL of tetrahydrofuran (THF) were loaded into the autoclave and sealed. After purged five times with H_2, the reactor was pressurized with H_2 to 1.4 MPa pressure at room temperature. Then, the reactor was heated to 180 °C and maintained for 4 hours at 400 rpm. When the time is due, the reaction was quenched immediately with cold water. The liquid mixture obtained was mixed with a given amount of tetradecane as an inert internal standard, diluted with solvent, and then filtered using a 0.2 mm syringe filter to remove the catalyst for compositional analysis by GC. The recycle studies were carried out as follows. After each catalytic run, the reaction mixture was allowed to settle, and the clear supernatant liquid containing product was removed from the reactor. Next, the catalyst was washed with THF two times by redispersion, settling and removal of the supernatant liquid. Finally, the catalyst residue retained in the reactor was used for the next run without drying and calcination.

The products were analyzed by a gas chromatograph (GC HP7820) with flame ionization detector (FID) using a PEG2W capillary column and H_2 as a carrier gas. The results were quantified as LA conversion (C_{LA}), GVL selectivity (S_{GVL}) and yield (Y_{GVL}) in mol.% on the basis of initial molar amount of LA. Repeated runs showed that data variation was in the range of ± 2% (relative value). Overall carbon balance in the products was > 98%.

Table 1

Metal leaching and catalytic properties of Cu- and/or Ag-containing catalyst for hydrogenation of LA into GVL.[a]

Entry	Catalyst	Catalyst preparation conditions	Reaction conditions			C_{LA} (mol.%)	S_{GVL} (mol.%)	Leaching (ppm)	
			T/°C	p/MPa	t/h			Cu	Ag
1	CuO powder[b]	Cu(OH)$_2$ calcined at 450 °C in air for 3 h	180	1.4	4	–	–	176.5	–
2	Metal Cu powder[b]	CuO reduced at 350 °C in 5% H$_2$/Ar for 2 h	180	1.4	4	–	–	0.1	–
3	Cu$_{0.8}$/Al$_2$O$_3$	Calcined at 450 °C in air for 3 h	180	1.4	4	3	97	73.8	–
4	Cu$_{0.8}$/Al$_2$O$_3$-H$_2$	Cu$_{0.8}$/Al$_2$O$_3$ reduced at 350 °C in 5% H$_2$/Ar for 2 h	180	1.4	4	100	> 99	33.0	–
5	Cu$_{0.8}$/Al$_2$O$_3$-H$_2$	Cu$_{0.8}$/Al$_2$O$_3$ reduced at 350 °C in 5% H$_2$/Ar for 2 h	180	4.0	4	100	92	5.8	–
6	Cu$_{0.8}$/Al$_2$O$_3$-H$_2$	Cu$_{0.8}$/Al$_2$O$_3$ reduced at 350 °C in 5% H$_2$/Ar for 2 h	265	1.4	4	100	87	0.9	–
7	Cu$_{0.8}$Ag$_{0.8}$/Al$_2$O$_3$	Calcined at 450 °C in air for 3 h	180	1.4	4	100	> 99	< 0.1	ND
8	Ag$_{0.8}$/Al$_2$O$_3$	Calcined at 450 °C in air for 3 h	180	1.4	4	31	99	–	ND

ND = not detected.

[a] Reaction conditions: 300 mg of LA in 6 mL of THF; catalyst loading = 150 mg.

[b] Catalyst loading: Cu amount equals to Cu molar quantity in the Cu$_{0.8}$/Al$_2$O$_3$ catalyst.

3. Results and discussion

3.1. Investigation of metal leaching and catalytic activity

A series of Cu- and/or Ag-containing catalysts were prepared for the hydrogenation of LA, and metal leaching was studied by ICP-OES analysis (Table 1). As shown in Table 1, the extent of Cu metal leaching distinctly changed with catalyst compositions and reaction conditions. Cu leaching reached the maximum (176.5 ppm) for CuO but was only 0.1 ppm for metal Cu powder. This result indicates the formation of a soluble copper carboxylate complex through the reaction of LA with Cu in the oxidation state rather than in the metal state. Therefore, severe metal leaching reaching 73.8 ppm was detected in the Cu catalyst without pre-reduction (Cu$_{0.8}$/Al$_2$O$_3$) (Entry 3 in Table 1). The catalyst also showed minimal activity in catalyzing LA hydrogenation, despite its high selectivity to GVL. Meanwhile, under the same reaction condition, leaching reached 33.0 ppm in the case of the Cu$_{0.8}$/Al$_2$O$_3$-H$_2$ catalyst reduced at 350 °C in 5 vol.% H$_2$/Ar for 2 h. The highly dispersed Cu particles on the support may exhibit some properties that differ from the isolated Cu metallic particles since Cu leaching from Cu$_{0.8}$/Al$_2$O$_3$-H$_2$ cannot be ignored. Although the reaction in Entry 4 led to the complete conversion of LA with almost 100 mol.% selectivity to GVL, the use of Cu$_{0.8}$/Al$_2$O$_3$-H$_2$ remains challenging because of severe metal leaching under mild reaction conditions. In a similar study, Hengne et al. reported that Cu leaching reached 174 ppm for Cu-Al$_2$O$_3$ catalyst prepared by coprecipitation and reduced under H$_2$ pressure during the complete conversion of LA in water at 200 °C and 500 psi H$_2$ [25]. Table 1 (Entries 5 and 6) shows that the metal leaching of Cu$_{0.8}$/Al$_2$O$_3$–H$_2$ was extensively suppressed in the reaction at high temperature or H$_2$ pressure, which is in agreement with previous reports that few Cu leached in reactions over Cu catalysts at 265 °C [27] or under 7 MPa H$_2$ [28]. The selectivity to GVL decreased to 92 mol.% and 87 mol.% during the reaction at 180 °C/4.0 MPa H$_2$ and at 265 °C/1.4 MPa H$_2$, respectively. The hydrogenation of LA over Cu$_{0.8}$/Al$_2$O$_3$-H$_2$ at 180 °C/4.0 MPa H$_2$ formed GVL as major product and 1,4-pentanediol and 2-methyltetrahydrofuran as minor products. In the reaction at 265 °C/1.4 MPa H$_2$, the reaction solvent exhibited light yellow color possibly because of humins, which cannot be detected by GC. Therefore, harsh reaction conditions can overcome the problem of Cu leaching to a certain extent at the expense of sacrificing GVL selectivity and high energy consumption. For the Cu$_{0.8}$Ag$_{0.8}$/Al$_2$O$_3$ catalyst, no metal leaching was observed despite conducting the reaction at low temperature (180 °C) and H$_2$ pressure (1.4 MPa). Moreover, the Cu$_{0.8}$Ag$_{0.8}$/Al$_2$O$_3$ catalyst without reduction pretreatment led to the complete conversion of LA and > 99 mol.% selectivity to GVL under mild reaction conditions. The Ag$_{0.8}$/Al$_2$O$_3$ catalyst exhibited catalytic activity without Ag leaching. The sum of the conversions of Cu$_{0.8}$/Al$_2$O$_3$ (Entry 3) and Ag$_{0.8}$/Al$_2$O$_3$ (Entry 8) did not generate comparable result as that of Cu$_{0.8}$Ag$_{0.8}$/Al$_2$O$_3$. Therefore, CuAg/Al$_2$O$_3$ can be prepared

without the high-temperature reduction as pretreatment, and Ag effectively eliminates Cu leaching from the catalyst under mild reaction conditions. CuAg/Al$_2$O$_3$ is thus considered an eco-friendly catalyst for efficient hydrogenation of LA into GVL.

The reusability of Cu$_{0.8}$Ag$_{0.8}$/Al$_2$O$_3$ in the hydrogenation of LA into GVL was investigated and compared with that of Cu$_{1.6}$/Al$_2$O$_3$-H$_2$. After the first hydrogenation, the catalyst was recovered from the reaction mixture and directly used for subsequent run without drying or calcination. This procedure was conducted several times, and the results are shown in Fig. 1. The catalytic performance of the Cu$_{0.8}$Ag$_{0.8}$/Al$_2$O$_3$ catalyst remained almost the same after nine successive runs, indicating its good stability. The recycled Cu$_{1.6}$/Al$_2$O$_3$-H$_2$ catalyst showed relatively good activity, slightly decreased the LA conversion rate after three recycles, and was rapidly deactivated starting at the fourth recycle. The clear supernatant product from each reaction over Cu$_{1.6}$/Al$_2$O$_3$-H$_2$ is blue in color, which intensified during the fourth and fifth recycles. This finding suggests that Cu leaching is one of the major factors that deactivate Cu$_{1.6}$/Al$_2$O$_3$-H$_2$. In the case of the Cu$_{0.8}$Ag$_{0.8}$/Al$_2$O$_3$ catalyst, Cu leaching was completely suppressed, as evident by the colorless transparent liquid product, the ICP-OES analysis results, and the good recyclability in successive runs. The TGA profile (Fig. S1) of the spent Cu$_{0.8}$Ag$_{0.8}$/Al$_2$O$_3$ catalyst did not show weight loss at temperatures higher than 500 °C, indicating that no coke was deposited on the catalyst during the hydrogenation of LA under mild conditions.

The effects of catalyst preparation and reaction conditions were studied in detail and the results were shown in Supporting Information. The CuAg/Al$_2$O$_3$ catalysts with the same total metal loading (1.6 mmol Cu and Ag per gram γ-Al$_2$O$_3$) but different molar ratios of Cu to Ag were
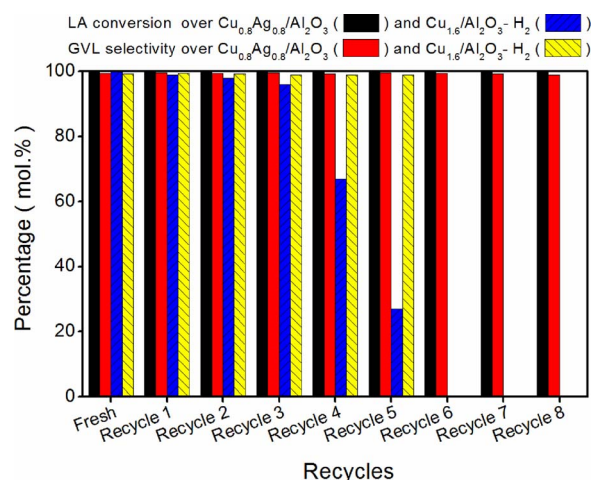

Fig. 1. Reuse of Cu$_{0.8}$Ag$_{0.8}$/Al$_2$O$_3$ and Cu$_{1.6}$/Al$_2$O$_3$-H$_2$ catalysts (reaction conditions: 300 mg of LA in 6 mL of THF solvent, catalyst loading = 150 mg, 180 °C, 1.4 MPa H$_2$, and 4 h).

prepared and tested for the hydrogenation of LA. The reaction results were shown in Fig. S2, and the metal leaching results were summarized in Table S1. $Cu_{1.6}/Al_2O_3$ only presents a LA conversion of 4 mol.% at 180 °C, 1.4 MPa H_2 and 3 h reaction; with replacement of 20% of Cu by Ag, the LA conversion increases sharply to 77 mol.%; the maximal conversion of 85 mol.% is achieved on $Cu_{0.8}Ag_{0.8}/Al_2O_3$ under the same reaction condition. Complete replacement of Cu by Ag, namely, $Ag_{1.6}/Al_2O_3$, exhibits good activity but is not comparable to the bimetallic catalysts. As shown in Table S1, the quantity of Cu leaching reaches 111.9 ppm for $Cu_{1.6}/Al_2O_3$, but significantly decreases for the catalysts with Ag participation. Cu leaching is weakened with the increase of Ag content in the CuAg bimetallic catalysts, and is thoroughly suppressed in the case of the $Cu_{0.8}Ag_{0.8}/Al_2O_3$ catalyst. Ag is not leached either in the Ag monometallic catalyst or in the CuAg bimetallic catalysts. Regardless of the Cu to Ag molar ratios on these supported catalysts, the selectivity to GVL always exceeds 97 mol.%. The results of reaction on $Cu_{0.8}Ag_{0.8}/Al_2O_3$ catalysts with different metal loadings (molar ratio of Cu:Ag is fixed at 1:1, Fig. S3a) shows volcano-type dependence on CuAg loading. The LA conversion increased rapidly with increasing CuAg amount from 0.4 mmol to 1.6 mmol per gram of γ-Al_2O_3, began to increase slowly until 3.2 mmol per gram of γ-Al_2O_3, and declined from that point. The selectivity toward GVL remained constant around 99 mol.% regardless of metal loading in the range studied. A steady decrease in surface area and pore volume was observed with the increase in CuAg loading according to the N_2 adsorption results of CuAg/Al_2O_3 (Fig. S3b). The lower efficiency of the CuAg at higher metal loadings can be explained by a decrease of CuAg dispersion at elevated loading. The catalyst loading at 1.6 mmol per gram of γ-Al_2O_3 provides sufficient metallic sites with a good metal dispersion, thus presenting the highest efficiency for LA conversion. Increasing reaction temperature from 170 °C to 200 °C exerts an increasing conversion of LA, but the GVL selectivity remains at nearly ~99 mol.% and does not decrease even at 220 °C (Fig. S4a). With the increase in H_2 pressure in the range of 0.8–2.5 MPa, LA conversion increased rapidly and reached 100 mol.% at 2.5 MPa after 0.5 h (Fig. S4b). The GVL selectivity is independent of H_2 pressure and remains at almost 99 mol.% even at a high pressure of 4.5 MPa. The influence of solvent on LA conversion was investigated, and the results are reported in Table S2. The THF solvent with the most suitable polarity exhibits balanced hydrophilic/hydrophobic property that benefits the adsorption of reactants and desorption of the product. The low boiling point of THF (66 °C) facilities the recovery of GVL (boiling point, 208 °C) through distillation of the solvent. The conversion of LA in water cannot be compared with that in THF under similar experimental conditions. Only 8 mol.% of LA was converted in water under mild conditions of 180 °C and 1.4 MPa H_2 after 2 h. A small amount of 4-hydroxypentanoic acid as byproduct could be detected during reaction in water.

3.2. Characterization of $Cu_{0.8}Ag_{0.8}/Al_2O_3$

XPS measurements of fresh and spent $Cu_{0.8}Ag_{0.8}/Al_2O_3$ were performed to identify the chemical state of Cu and Ag in the samples (Fig. 2). The whole XPS survey profiles of the fresh and spent catalysts (Fig. S5) present the elements of Cu, Ag, Al and O. The difference in the binding energy between Cu° and Cu$^+$ is only 0.1 eV and cannot be distinguished [34], so the spin–orbit split peaks of Cu species at 952.5 ($2p_{1/2}$) and 932.3 eV ($2p_{3/2}$) are attributed to Cu° or Cu$^+$. The XPS spectra of fully oxidized Cu^{2+} species shifted to higher binding energies at 953.8 ($2p_{1/2}$) and 933.5 eV ($2p_{3/2}$), and satellite peaks were detected at around 963 and 943 eV [34]. The spin–orbit split peaks of Ag $3d_{3/2}$ and Ag $3d_{5/2}$ at 374.0–374.3 ($3d_{3/2}$) and 368.0–368.3 eV ($3d_{5/2}$), respectively, are characteristics of metal Ag [34,35]. The Gaussian fitting of the Cu $2p$ binding energy region shows that fresh $Cu_{0.8}Ag_{0.8}/Al_2O_3$ calcined at 450 °C in air mainly contains Cu^{2+} and a few Cu°/Cu$^+$ species. The satellite peaks of the fresh catalyst further confirms the presence of CuO on its surface. The Ag $3d$ signals of the fresh catalyst at 368.3 and 374.3 eV indicate the metallic state of Ag species. The broadening of peak width cannot be related to Ag oxides because the peaks of Ag species in the oxidation state shifted to lower binding energies, below 374.0 ($3d_{3/2}$) and 368.0 eV ($3d_{5/2}$), respectively [34]. This result could be due to the close interaction of well-dispersed Ag nanoparticles with the support substrate [35]. Seery et al. [36] reported that Ag_2O on the TiO_2 surface was decomposed to metallic Ag when calcined at temperatures higher than 400 °C. Another study stated the occurrence of the photoreduction of the Ag-Cu/TiO_2 catalyst under natural and artificial light [37]. In the present study, the $Cu_{0.8}Ag_{0.8}/Al_2O_3$ catalyst was calcined at 450 °C and exposed to light during preparation and storage, so the XPS spectra reveal the presence of metallic Ag in the fresh $Cu_{0.8}Ag_{0.8}/Al_2O_3$ catalyst. Ag/Al_2O_3 with high Ag loading partly remains in the oxidation state [31]. Because Cu clusters are sensitive to oxygen and prone to be oxidized rapidly in air, the spectra show the existence of fully oxidized Cu^{2+} species on Cu/Al_2O_3 [31]. But a portion of Cu species in $Cu_{0.8}Ag_{0.8}/Al_2O_3$ exists in the low valence state, namely, Cu$^+$ or Cu°. Thus, Ag partly reduces Cu even in the fresh catalyst. The extent of the effect of Ag depends on the ratio of Cu to Ag, considering that few reduced Cu species were detected in the sample with a high Cu to Ag molar ratio of 7:3 [31]. After one reaction cycle at 180 °C in the presence of hydrogen, the Cu $2p$ signals slightly shifted to lower binding energies (952.5 and 932.3 eV), and the satellite peaks diminished significantly. This finding indicates that the CuO component that existed originally in the fresh catalyst was reduced in the reaction system. During the reaction, the bimetallic catalyst underwent in situ reduction. The binding energy difference between Cu° and Cu$^+$ is only 0.1 eV [34], so the Cu $2p$ signals of the spent catalyst cannot distinguish the two states. The spent catalyst (collected by washing and vacuum drying) showed nearly no reduction peak in H_2-TPR analysis (data not shown here), indicating that Cu remained in the metallic state in the spent catalyst. According to the Ag $3d$ signal
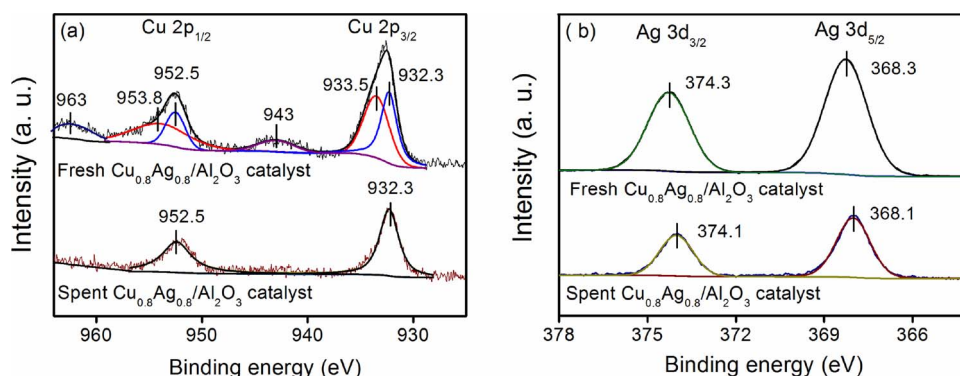

Fig. 2. XPS spectra in the binding energy range of (a) Cu $2p$ and (b) Ag $3d$ of fresh and spent $Cu_{0.8}Ag_{0.8}/Al_2O_3$.

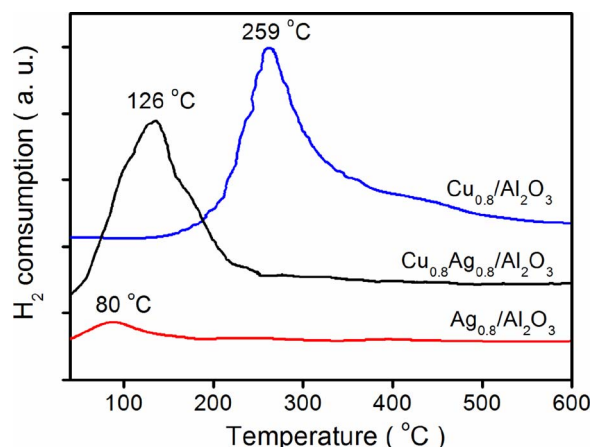**Fig. 3.** TPR patterns of Cu- and Ag-supported catalysts including $Cu_{0.8}/Al_2O_3$, $Cu_{0.8}Ag_{0.8}/Al_2O_3$, and $Ag_{0.8}/Al_2O_3$.

results, Ag also remained in the metallic state in the spent catalyst.

The TPR patterns of Cu- and Ag-supported catalysts are presented in Fig. 3. $Cu_{0.8}/Al_2O_3$ displayed a peak centered at 259 °C, which corresponds to the reduction of CuO on γ-Al_2O_3 [32]. $Ag_{0.8}/Al_2O_3$ showed nearly no reduction peak, which is consistent with the XPS results and confirms that Ag is in the metallic state in the fresh catalyst. The TPR pattern of the $Cu_{0.8}Ag_{0.8}/Al_2O_3$ catalyst contains a broad major peak at around 126 °C and two shoulders ahead and behind the major peak. The major peak of the sample with Cu to Ag molar ratio of 7:3 is around 150 °C [31]. Thus, increasing the relative content of Ag favorably decreases the reduction temperature of the catalyst. The shoulder from the low-temperature region around 110 °C belongs to the easily reducible Cu^{2+}/Cu^+ with small size or is related to Ag-rich clusters. The high-temperature shoulder peak is assigned to large-sized CuO particles or possibly due to insufficient Ag participation. The reduction peak of Cu in $Cu_{0.8}Ag_{0.8}/Al_2O_3$ is 133 °C lower than that in $Cu_{0.8}/Al_2O_3$. Based on the reduction profiles of the catalysts, Ag exhibits strong effect on Cu reduction behavior. The TPR patterns of $CuAg/Al_2O_3$ catalysts with different ratios of Cu to Ag (Fig. S6) further confirms the strong effect of Ag content on the reduction temperature of CuO. The reduction peaks of the CuO crystallite on the catalyst surface shift to lower temperature with increasing Ag content of the bimetallic catalysts.

Fig. 4(a) and (b) shows the TEM images of $Cu_{0.8}Ag_{0.8}/Al_2O_3$ before and after the reaction at 180 °C and 1.4 MPa H_2, respectively. Fresh catalyst was prepared through calcination at 450 °C in the air, and its TEM images (Fig. 4a) show the homogenous dispersion of metallic species with ultrafine nanoparticles and clusters. The $Cu_{0.8}Ag_{0.8}/Al_2O_3$ catalyst underwent two processes during the first run in the reaction: in situ reduction of metal oxides on the catalyst surface and catalysis for hydrogenation of LA into GVL. The metal oxides on the support surface after reduction treatment usually form small metal particles with sizes of tens of nanometers depending on catalyst preparation and reduction conditions; that is, the particle size may increase and vary widely in the spent catalyst because of the sintering of metallic nanoparticles [25,38]. Particles on the spent catalyst surface show similar size and morphology and narrow size distribution (Fig. 4b). The particle sizes range from 2 nm to 14 nm, with an average of 6 nm. The slight sintering of metal species after the reaction did not destroy the catalyst structure, as indicated by slight decrease in the specific surface area (204 $m^2\,g^{-1}$ for the fresh catalyst and 197 $m^2\,g^{-1}$ for the spent catalyst) and pore volume (0.27 $cm^3\,g^{-1}$ for the fresh catalyst and 0.25 $cm^3\,g^{-1}$ for the spent catalyst). The $Cu_{0.8}Ag_{0.8}/Al_2O_3$ catalyst was specially reduced in 5 vol. % H_2/Ar at 180 °C for 4 h under temperature and time conditions similar to those in the reaction to determine the difference between in situ reduction and conventional reduction methods. The TEM image (Fig. 4c) shows that the particle sizes of the sample reduced in H_2 gas

range from 10 nm to 38 nm, with an average of 20 nm, which is larger than that of the spent catalyst (Fig. 4b), and is even larger than that of the catalyst after nine successive cycles (Fig. S7). Hence, metal sintering of the catalyst reduced in H_2/Ar is more severe than that of the reduced catalyst in the reaction solvent in situ. Therefore, the good stability of the $Cu_{0.8}Ag_{0.8}/Al_2O_3$ catalyst over repeated cycles is partly due to the slight sintering of the active sites in the in situ reduction of the catalyst under mild reaction conditions.

The spent $Cu_{0.8}Ag_{0.8}/Al_2O_3$ catalyst samples were analyzed by HRTEM (Fig. 4d). Cu and Ag did not form flawlessly-ordered alloy phases; the Cu-Ag system exhibits a tendency for phase separation due to the large difference in their atom size (Cu is smaller than Ag by 12%) and cohesive energy ($E_{coh\,Ag} - E_{coh\,Cu} = 0.55\,eV$) [39]. At present, the XRD spectrum of Cu-Ag alloy has not been indexed to the JCPDS PDF Card database; hence, this alloy is not an easily available compound with precise crystal structure. Previous studies reported that Cu and Ag can form alloy or colloid under mild conditions. For example, Ag-Cu alloy nanoparticles were synthesized by light irradiation [37,39] or by reduction with hydrazine and citric acid as stabilizer [40]. Wei et al. [41] deduced three metastable ordered phases, namely, $CuAg_3$, $CuAg$, and Cu_3Ag, in the phase diagram of Cu-Ag below the 230 °C region. The configurations of Cu-Ag particles include core-shells (Cu core-Ag shell or Ag core-Cu shell) and clusters (colloids of Cu and Ag small clusters or abundant one cluster with the other as impurity) [35–41]. Whatever structure, Cu and Ag can form a strong interplay of geometric and electronic effects [35,39–41]. In the present study, the $Cu_{0.8}Ag_{0.8}/Al_2O_3$ catalyst was reduced in situ under mild conditions (180 °C, 1.4 MPa H_2). After the in situ reduction of the bimetallic catalyst, Cu and Ag underwent self-assembly to form bimetallic Cu-Ag nanoparticles. When some Cu atoms in the Cu lattice are substituted with Ag atoms, the bonds in the lattice will swell and increase in size because they are connecting larger Ag atoms, and vice versa [40]. The interplanar spacings of 0.208 and 0.236 nm correspond to the (111) plane of pure metal Cu (JCPDS PDF Card No.: 04-0836) and Ag (JCPDS PDF Card No.: 04-0783), respectively. The interplanar spacings of the metal nanoparticles on the spent catalyst were measured in several HRTEM images (Fig. 4d, Fig. S8). All the images show irregular particle morphology with short-ranged ordered structure and long-ranged disorder. The lattice fringes represent the average values of the local regions because of the distortion and discontinuity of the crystal lattice (see magnified image of lattice fringe in Fig. 4d). Most of the lattice fringe distances of the particles are located between pure Ag (111) and pure Cu (111) planes. In Fig. 4d, the smaller lattice fringes of 0.209 and 0.210 nm approach the (111) plane of pure metal Cu, and the larger lattice fringes of 0.231 and 0.236 nm are close or equal to the (111) plane of pure metal Ag. The presence of Cu-Ag nanoparticles in cluster form or in core-shell form on γ-Al_2O_3 was confirmed by the HRTEM images of the spent catalyst. Almost each nanoparticle simultaneously includes the interplanar spacings close to the Cu (111) and the Ag (111) lattice fringes, which means that both Cu and Ag present on the surface of the nanoparticles. Therefore, the two metals are in cluster form on γ-Al_2O_3. These results indicate the co-existence and close proximity of Ag and Cu atoms in the particles on the γ-Al_2O_3 surface.

Fig. 5 displays the elemental distribution maps of Ag, Cu, Al, and O in the spent catalyst. The STEM image of the spent $Cu_{0.8}Ag_{0.8}/Al_2O_3$ catalyst shows nanoparticles attached on the γ-Al_2O_3 surface (Fig. 5a). The mappings demonstrate the non-homogeneous dispersion of Cu (Fig. 5b) and Ag (Fig. 5c) atoms and the even and dense distribution of Al (Fig. 5d) and O (Fig. 5e) on the catalyst surface. When tracing the same particle from Fig. 5a to Figs. 5b and c, each particle contains both Cu and Ag. Hence, Cu and Ag assembled together to form clusters during the in situ reduction, which is consistent with the HRTEM results. The nonuniformity of Cu–Ag distribution on the catalyst is in accordance with the Cu reduction property (Fig. 3).

The XRD patterns of the fresh and spent $Cu_{0.8}Ag_{0.8}/Al_2O_3$ catalysts were analyzed (Fig. 6). Only the reflection of the γ-Al_2O_3 crystalline

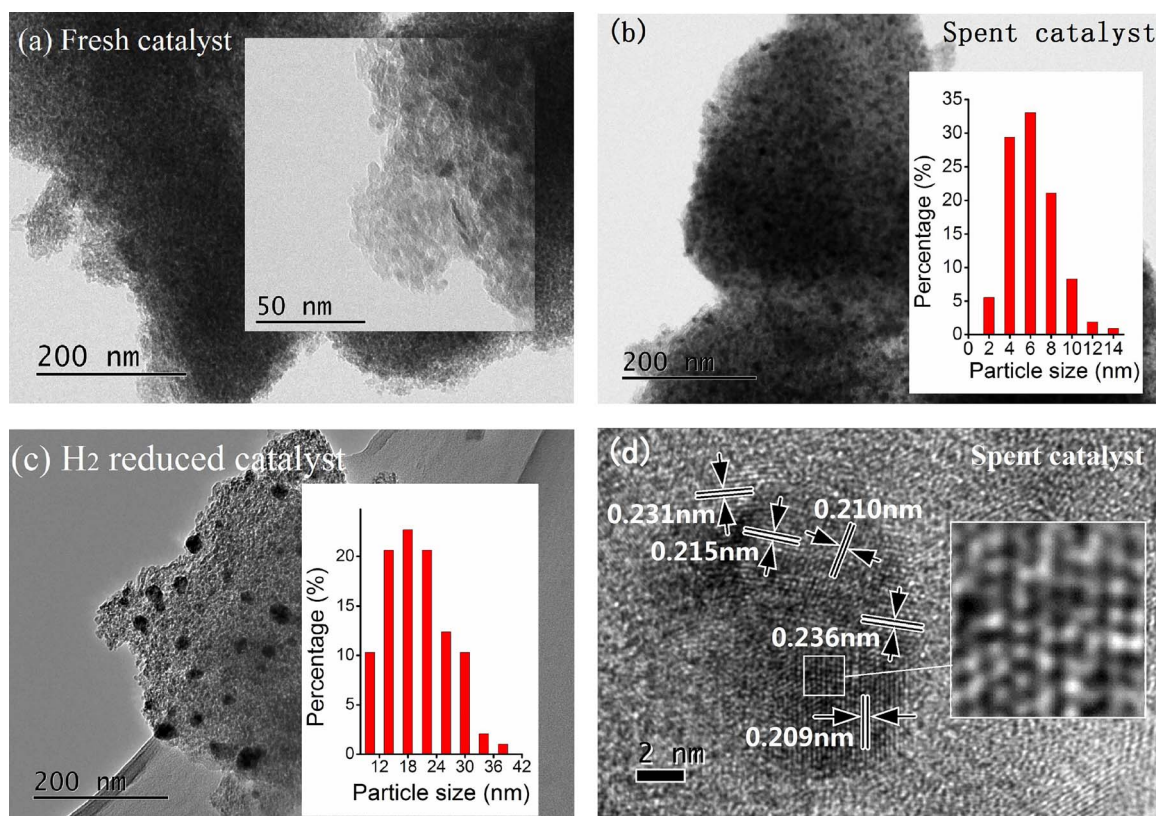**Fig. 4.** TEM and HRTEM images of $Cu_{0.8}Ag_{0.8}/Al_2O_3$ including (a) TEM of the fresh catalyst, (b) TEM of spent catalyst, (c) TEM of the H_2 reduced catalyst, and (d) HRTEM image of the spent catalyst.

(JCPDS PDF Card No.: 50-741) was found in the XRD signals of the fresh catalyst. The absence of the diffraction peaks attributed to Ag and Cu phases may be due to small crystalline sizes, which were below the detection limit of the XRD technique. Although the spent catalyst formed nanoparticles (Fig. 4b), the diffraction lines corresponding to Ag and Cu were not evident even in the catalyst after nine successive runs (Fig. S9). Several weak diffraction peaks of Ag, such as (111), (220), and (331) peaks, were detected. The peak around 2 theta of 38° is the result of the overlapping reflection signals between Ag (111) and γ-Al_2O_3 [(311) and (222)], with the Ag (111) peak at the top position. The XRD results were used to confirm the formation of Ag-Cu alloy

species [37]. The XRD results did not show the precise diffraction lines attributed to Ag-Cu alloy. However, the widened Ag (111) peak and the low-intensive signals attributed to Ag and Cu manifest the weak crystallinity of the metals. The close proximity and the strong interaction between Ag and Cu enhance the amorphization of crystallites. This conclusion is in accord with the less regular morphology of the particles shown in Fig. 4d.

3.3. Mechanism discussions

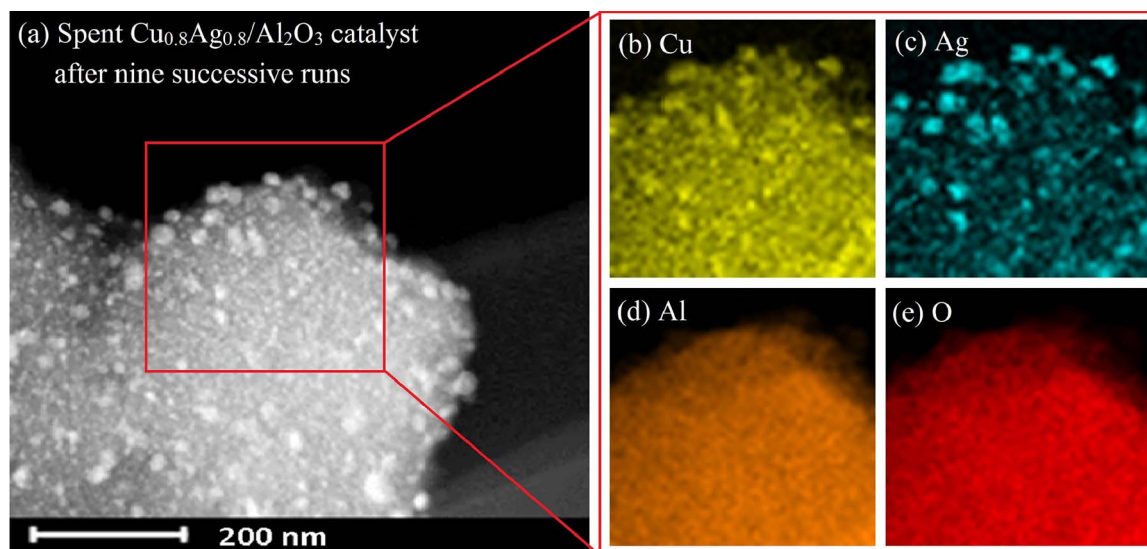Scheme 1 shows the possible mechanisms for in situ reduction and

Fig. 5. Elemental map of the spent $Cu_{0.8}Ag_{0.8}/Al_2O_3$ catalyst obtained by STEM-EDS: (a) STEM image; (b) Cu channel; (c) Ag channel; (d) Al channel; and (e) O channel.
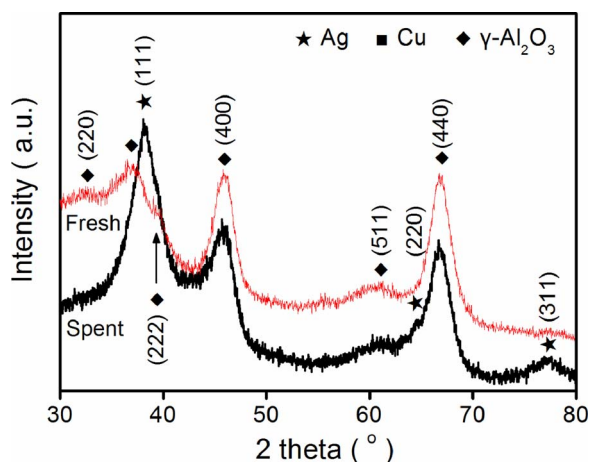
Fig. 6. XRD patterns of the fresh and spent $Cu_{0.8}Ag_{0.8}/Al_2O_3$ catalysts.

for prevention of metal leaching as well as the reaction pathway. The in situ reduction of the $Cu_{0.8}Ag_{0.8}/Al_2O_3$ catalyst during the reaction could be due to hydrogen spillover [31]. The Cu monometallic catalyst, $Cu_{0.8}/Al_2O_3$, cannot be reduced in situ under the reaction conditions of 180 °C and 1.4 MPa H_2, as indicated by the poor reaction performance and severe leaching of Cu (Entry 3 in Table1) as well as the blue color in the reaction solvent. By contrast, $Cu_{0.8}Ag_{0.8}/Al_2O_3$ was effectively reduced under the same conditions. In the case of the $Cu_{0.8}Ag_{0.8}/Al_2O_3$ catalyst during the reaction, Ag species with very low reduction temperature exist in the metallic state. In the beginning of the reaction, molecular hydrogen first splits into hydrogen atoms via dissociative chemisorption on Ag active sites, followed by the migration of H atoms from the Ag sites onto neighboring CuO sites. H atoms subsequently reduce CuO into metallic Cu species. This deduction shows that hydrogen spillover from Ag plays a critical role in the in situ reduction of the catalyst during the reaction. However, the effect of hydrogen spillover cannot cover the critical role of Ag in preventing Cu leaching. Otherwise, Cu leaching from the $Cu_{0.8}/Al_2O_3$-H_2 catalyst cannot occur because the catalyst itself can generate hydrogen spillover from the reduced Cu sites. Therefore, hydrogen spillover during the reaction is not a valid solution to solve the problem of metal leaching.

Table 1 shows that the leached Cu is from the metal in the oxidation state rather than in the metal state. The reason for Cu leaching from $Cu_{0.8}/Al_2O_3$-H_2 is probably because of Cu reoxidation during the reaction. Metal reoxidation occurs in some reaction conditions even with H_2 participation [27,42]. Putrakumar et al. [27] studied the hydrogenation of LA to GVL over Cu catalysts supported on γ-Al_2O_3 and found that Cu oxides were formed in the spent catalyst due to the reoxidation of Cu on the supports. Hilmen et al. [42] reported that the reoxidation of Co/Al_2O_3 led to deactivation when the catalyst was

exposed to H_2O/H_2 during Fischer–Tropsch synthesis; the reoxidation rate increases with decreasing H_2 pressure. In the present study, the reaction temperature and H_2 pressure were set as 180 °C and 1.4 MPa, respectively, and H_2O was formed as byproduct in the system. In this case, the gradual reoxidation of Cu followed by Cu leaching is unavoidable in the $Cu_{0.8}/Al_2O_3$-H_2 catalyst. This inference was confirmed by designing and conducting several experiments using water (Table 2).

Fresh $Cu_{0.8}/Al_2O_3$ catalyst exhibits blue color (Fig. 7a), and the $Cu_{0.8}/Al_2O_3$-H_2 catalyst shows black color (Fig. 7b). The spent $Cu_{0.8}/Al_2O_3$-H_2 catalyst reacted in water is yellow color (Fig. 7c), and almost no Cu was leached in the water (Entry 1 in Table 2). The catalyst reacted in water containing LA is gray (Fig. 7d), and the reaction was accompanied by severe Cu leaching (Entry 2 in Table 2). XPS measurements identified the chemical states of Cu in the spent $Cu_{0.8}/Al_2O_3$-H_2 catalysts reacted in water and water containing LA the samples (Fig. S10). After the reaction at 180 °C in water, the Cu $2p$ signals of the spent $Cu_{0.8}/Al_2O_3$-H_2 sample show binding energies at 952.5 and 932.4 eV without accompanying satellite peaks, indicating the elimination of the Cu^{2+} component. The TPR pattern of the sample clearly displayed a peak within the 200 °C–320 °C range (Fig. S11), indicating that Cu is in the oxidation state rather than in the metallic state in the spent catalyst. After reaction at 180 °C in water containing LA, the XPS peak intensity of the sample is much weak compared with that after reaction in water, manifesting the insufficiency of the Cu species on the γ-Al_2O_3 surface. The remaining Cu species is Cu(s) according to the Cu $2p$ binding energies and the gray color of the sample. Considering these observations, we conclude that after reaction in water, the metallic Cu species originally present in the $Cu_{0.8}/Al_2O_3$-H_2 catalyst were oxidized into cuprous species, such as Cu_2O or CuOH, which is yellow and almost insoluble in water. Under the condition of water containing LA, two Cu^+ were transformed into Cu^{2+} and Cu(s) through disproportionation reaction $(2Cu^+ + 2H^+ \rightarrow Cu^{2+} + Cu(s) + H_2O)$. Cu^{2+} further forms water-soluble complex with LA and water molecules. Thus, severe Cu leaching occurred in water containing LA. H_2 leads to the reduction of the Cu components, and a high temperature makes H_2 work well. Therefore, few Cu species leached in the reactions over Cu catalysts at a high temperature (265 °C) [27] or H_2 pressure (7 MPa H_2) [28]. However, the reoxidation of Cu was not suppressed when conducting the reaction at a low temperature (180 °C) and H_2 pressure (1.4 MPa); thus, Cu leaching is severe (Entry 3 in Table 2).

$Cu_{0.8}Ag_{0.8}/Al_2O_3$ used in this study is the catalyst obtained after calcination in air, so most of the Cu species on the γ-Al_2O_3 surface are initially in the oxidation state. As described above, Cu leached from the species in the oxidation state. Notably, Cu can leach from $Cu_{0.8}Ag_{0.8}/Al_2O_3$ before it is reduced into metallic Cu in situ. A light blue color was observed during the reaction over $Cu_{0.8}Ag_{0.8}/Al_2O_3$ at 180 °C and 1.4 MPa H_2 in the THF solvent for 10 min, and the color disappeared when extending the reaction time to more than 1 h. The in situ reduction of $Cu_{0.8}Ag_{0.8}/Al_2O_3$ in water at 180 °C and 1.4 MPa H_2 takes longer
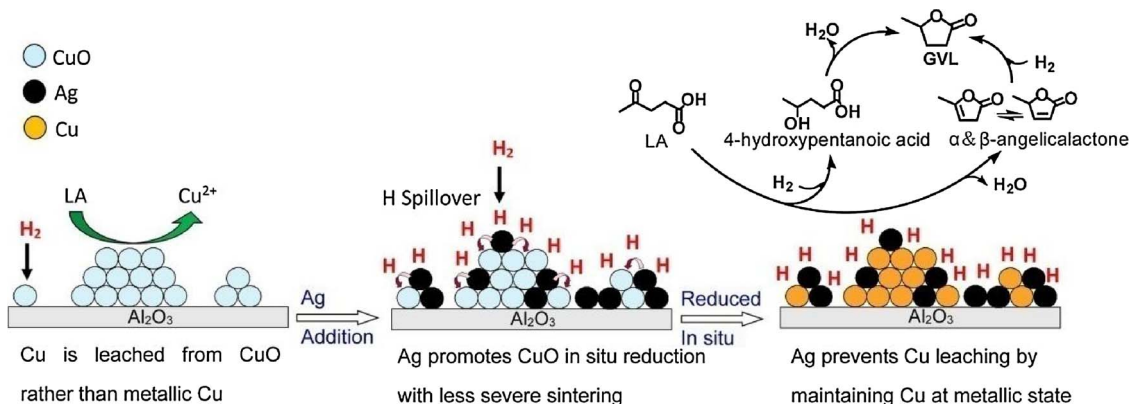
Scheme 1. Schematic of the proposed mechanisms of in situ reduction and metal leaching prevention and the reaction pathway.

Table 2
Metal leaching of the catalysts under different experimental conditions.

| Entry	Catalyst	Experimental conditions	Leaching (ppm)	
			Cu	Ag
1	$Cu_{0.8}/Al_2O_3$-H_2	6 mL of water, catalyst loading = 150 mg, 180 °C, 1.4 MPa N_2, and 1 h	0.4	–
2	$Cu_{0.8}/Al_2O_3$-H_2	300 mg of LA in 6 mL of water, catalyst loading = 150 mg, 180 °C, 1.4 MPa N_2, and 1 h	163.3	–
3	$Cu_{0.8}/Al_2O_3$-H_2	300 mg of LA in 6 mL of water, catalyst loading = 150 mg, 180 °C, 1.4 MPa H_2, and 1 h	114.1	–
4	$Cu_{0.8}Ag_{0.8}/Al_2O_3$	First, 150 mg of $Cu_{0.8}Ag_{0.8}/Al_2O_3$ was reduced in situ in 6 mL water at 210 °C, 4 MPa H_2, and 2 h. Then 300 mg of LA was added in the reactor followed by a reaction at 180 °C, 1.4 MPa H_2, and 1 h.	16.2	< 0.1
5	$Cu_{0.8}Ag_{0.8}/Al_2O_3$	First, 150 mg of $Cu_{0.8}Ag_{0.8}/Al_2O_3$ was reduced in situ in 6 mL water at 210 °C, 4 MPa H_2, and 2 h. Then 300 mg of LA was added in the reactor followed by a reaction at 200 °C, 3.4 MPa H_2, and 1 h.	1.7	< 0.1
6	Cu-Al_2O_3[a]	The catalysts were pre-reduced under H_2 at 300 °C for 12 h. Reaction conditions: 100 mL of LA water solution (5% w/w), catalyst loading = 0.5 g, 200 °C, 500 psi H_2, and 5 h.	174	–

[a] From reference [25].
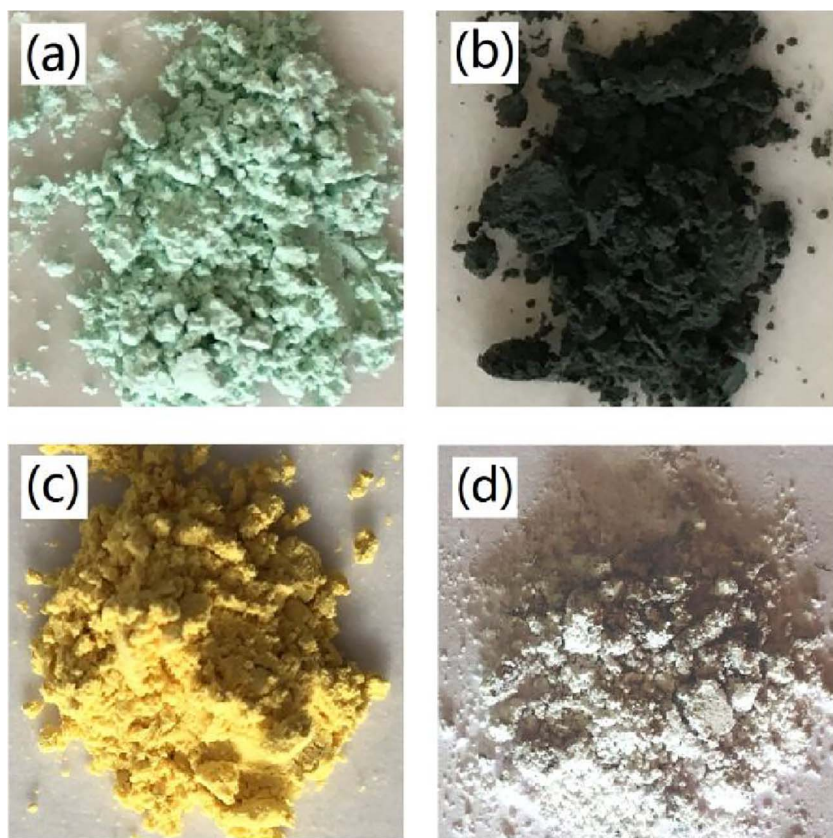
Fig. 7. Photos of the $Cu_{0.8}/Al_2O_3$ catalyst after various treatments: (a) fresh $Cu_{0.8}/Al_2O_3$ catalyst; (b) $Cu_{0.8}/Al_2O_3$-H_2 catalyst; (c) spent $Cu_{0.8}/Al_2O_3$-H_2 catalyst after reaction at 180 °C and 1.4 MPa N_2; and (d) spent $Cu_{0.8}/Al_2O_3$-H_2 catalyst after reaction in water containing LA at 180 °C and 1.4 MPa N_2. (For interpretation of the references to colour in text, the reader is referred to the web version of this article).

time than that in THF due to the low solubility of H_2 in water and the resistance of water in the reduction reaction. Regardless of the reduction rates of the Cu species, as long as Cu in $Cu_{0.8}Ag_{0.8}/Al_2O_3$ was reduced into the metallic state, Ag should ensure the prevention of the reoxidation of Cu during the reaction because it has special function to prevent Cu leaching. To shorten the reduction time, we reduced $Cu_{0.8}Ag_{0.8}/Al_2O_3$ in water at 210 °C and 4.0 MPa H_2 for 2 h. The reduced $Cu_{0.8}Ag_{0.8}/Al_2O_3$ catalyst ran a reaction in water containing LA (Entry 4 in Table 2) under the same conditions as those for the $Cu_{0.8}/Al_2O_3$-H_2 catalyst (Entry 3 in Table 2). Both the conversions of LA over the two catalysts were within 20 mol.%. The amount of Cu leached from the reduced $Cu_{0.8}Ag_{0.8}/Al_2O_3$ catalyst (16.2 ppm) is about a seventh of that from the $Cu_{0.8}/Al_2O_3$-H_2 catalyst (114.1 ppm). The Cu leaching amount decreased to 1.7 ppm when the reaction was performed over the reduced $Cu_{0.8}Ag_{0.8}/Al_2O_3$ catalyst at 200 °C and 3.4 MPa H_2 (Entry 5 in Table 2). Meanwhile, under the same reaction temperature (200 °C) and H_2 pressure (500 psi), the amount of Cu leached reached 174 ppm for the Cu-Al_2O_3 catalyst pre-reduced in a H_2 stream (Entry 6 in

Table 2) [25]. Cu leaching from the $Cu_{0.8}Ag_{0.8}/Al_2O_3$ catalyst was substantially suppressed compared with that from the $Cu_{0.8}/Al_2O_3$-H_2 catalyst or the Cu-Al_2O_3 catalyst under the same reaction conditions. This finding indicates that Cu in the bimetallic catalyst promoted by Ag exhibits distinct properties from that in the monometallic Cu catalyst.

Noble metal nanoparticles, such as Au and Ag, supported on TiO_2 surface can act as electron sink or trap media [43–45]. Ag is a cheap noble metal that possesses high electronic density of states [37]. Ag–Cu nanoparticles on TiO_2 or Ti substrates have been used in photocatalytic reactions [43,44]. The synergism between Ag and Cu allows them to act as electron traps; in this regard, Ag–Cu alloy nanoparticles possess high storage capacity to accumulate photoexcited electrons [37,43,44]. In the present study, the results of HRTEM and STEM/EDS mapping of $Cu_{0.8}Ag_{0.8}/Al_2O_3$ after the reaction reveal the coexistence of Cu and Ag in the nanoparticles. We believe that a strong geometric interplay between Cu and Ag causes strong electronic effects, including the formation of electron sinks or traps. The bimetallic nanoparticles in photocatalytic reactions collect photogenerated electrons, whereas those in

the present reaction accumulate the electrons donated by reductive agents such as H_2. Cu is prone to lie in the reduction state (metallic Cu) because the Cu–Ag nanoparticles on the $Cu_{0.8}Ag_{0.8}/Al_2O_3$ catalyst has high storage capacity of electrons; this finding was confirmed by the Cu 2p signals of the spent catalyst (Fig. 2a). Hence, the synergistic effect between Cu and Ag maintains Cu at metal state through accumulation of electrons and then significantly suppresses Cu leaching from the $Cu_{0.8}Ag_{0.8}/Al_2O_3$ catalyst.

The proposed reaction mechanisms occur in two routes based on reaction conditions, namely, hydrogenation of LA to 4-hydroxypentanoic acid followed by dehydrocyclization; or the dehydration of LA to angelicalactone and subsequent hydrogenation to produce GVL [3,4]. In our reactions over $CuAg/Al_2O_3$ in THF solvent, no intermediates were detected in the reactions conducted over a wide range of temperature, H_2 pressure, and duration. This finding could be due to the slow reaction steps for the formation of intermediates and subsequent fast steps. Both reaction routes over $CuAg/Al_2O_3$ involve a hydrogenation step on metal sites and a dehydration step on acid sites. Both Cu and Ag are responsible for hydrogenation. γ-Al_2O_3 acts as a good acidic support for the dehydration reaction. The combination of CuAg and γ-Al_2O_3 simultaneously achieves bifunctional catalytic activity with high selectivity toward GVL.

4. Conclusions

Using Ag to mediate Cu/Al_2O_3 catalysts exerts beneficial effects on the development of environment-friendly catalyst and economical and convenient processes for hydrogenation of LA into GVL. Under mild reaction conditions of 180 °C and 1.4 MPa H_2, Cu/Al_2O_3 suffered severe metal leaching even when it was thoroughly prereduced in 5 vol.% H_2/Ar. The addition of Ag to the Cu/Al_2O_3 catalyst significantly suppressed Cu leaching, thereby retaining the active sites of the catalyst and avoiding the contamination of the product. Moreover, Ag triggered the in situ reduction of Cu in $CuAg/Al_2O_3$ during the reaction. The in situ reduction of the catalyst led to less severe sintering of the active sites compared with external reduction by reducing gas. The characterization results confirmed the close proximity and the strong interplay in the geometric and electronic effects between Cu and Ag. Ag facilities Cu oxides reduction in situ through hydrogen spillover and prevents Cu leaching by maintaining Cu in the reduction state during the reaction. As a result, the $CuAg/Al_2O_3$ catalyst without reduction pretreatment led to the complete conversion of LA with approximately 100 mol.% selectivity to GVL at 180 °C under 1.4 MPa H_2 in THF solvent. After nine consecutive reactions, the catalyst retained its high catalytic activity and good stability without Cu leaching, coking, or notable sintering. The extensive elimination of metal leaching from the catalyst facilitates product purification and the proposed facile preparation method without high-temperature reduction can decrease the operation and maintenance costs; both of which contribute to clean and low-cost production of GVL.

Acknowledgements

Appendix A. Supplementary data

Supplementary material related to this article can be found, in the online version, at doi:https://doi.org/10.1016/j.apcatb.2018.03.033.

References

[1] D.M. Alonso, S.G. Wettstein, J.A. Dumesic, Bimetallic catalysts for upgrading of biomass to fuels and chemicals, Chem. Soc. Rev. 41 (2012) 8075–8098.

[2] H.B. Zhao, J.E. Holladay, H. Brown, Z.C. Zhang, Metal chlorides in ionic liquid solvents convert sugars to 5-hydroxymethylfurfural, Science 316 (2007) 1597–1600.

[3] K. Yan, Y. Yang, J. Chai, Y. Lu, Catalytic reactions of gamma-valerolactone: a platform to fuels and value-added chemicals, Appl. Catal. B: Environ. 179 (2015) 292–304.

[4] D.M. Alonso, S.G. Wettstein, J.A. Dumesic, Gamma-valerolactone, a sustainable platform molecule derived from lignocellulosic biomass, Green Chem. 15 (2013) 584–595.

[5] I.T. Horvath, H. Mehdi, V. Fabos, L. Boda, L.T. Mika, gamma-Valerolactone - a sustainable liquid for energy and carbon-based chemicals, Green Chem. 10 (2008) 238–242.

[6] J.S. Luterbacher, J.M. Rand, D.M. Alonso, J. Han, J.T. Youngquist, C.T. Maravelias, B.F. Pfleger, J.A. Dumesic, Nonenzymatic sugar production from biomass using biomass-derived gamma-valerolactone, Science 343 (2014) 277–280.

[7] B. Cai, X.C. Zhou, Y.C. Miao, J.Y. Luo, H. Pan, Y.B. Huang, Enhanced catalytic transfer hydrogenation of ethyl levulinate to γ-valerolactone over a robust Cu–Ni bimetallic catalyst, ACS Sustainable Chem. Eng. 5 (2016) 1322–1331.

[8] F. Li, L.J. France, Z. Cai, Y. Li, S. Liu, H. Lou, J. Long, X. Li, Catalytic transfer hydrogenation of butyl levulinate to γ-valerolactone over zirconium phosphates with adjustable Lewis and Brønsted acid sites, Appl. Catal. B: Environ. 214 (2017) 67–77.

[9] Y. Kuwahara, W. Kaburagi, Y. Osada, T. Fujitani, H. Yamashita, Catalytic transfer hydrogenation of biomass-derived levulinic acid and its esters to γ-valerolactone over ZrO₂ catalyst supported on SBA-15 silica, Catal. Today 281 (2017) 418–428.

[10] X. Tang, H. Chen, L. Hu, W. Hao, Y. Sun, X. Zeng, L. Lin, S. Liu, Conversion of biomass to γ-valerolactone by catalytic transfer hydrogenation of ethyl levulinate over metal hydroxides, Appl. Catal. B: Environ. 147 (2014) 827–834.

[11] J.A. Turner, Sustainable hydrogen production, Science 305 (2004) 972–974.

[12] V. Fábos, L.T. Mika, I.T. Horváth, Selective conversion of levulinic and formic acids to γ-valerolactone with the Shvo catalyst, Organometallics 33 (2014) 181–187.

[13] A.S. Piskun, J.E. de Haan, E. Wilbers, H.H. van de Bovenkamp, Z. Tang, H.J. Heeres, Hydrogenation of levulinic acid to γ-valerolactone in water using millimeter sized supported Ru catalysts in a packed bed reactor, ACS Sustainable Chem. Eng. 4 (2016) 2939–2950.

[14] A.S. Piskun, H.H. van de Bovenkamp, C.B. Rasrendra, J.G.M. Winkelman, H.J. Heeres, Kinetic modeling of levulinic acid hydrogenation to γ-valerolactone in water using a carbon supported Ru catalyst, Appl. Catal. A: Gen. 525 (2016) 158–167.

[15] S.G. Wettstein, J.Q. Bond, D.M. Alonso, H.N. Pham, A.K. Datye, J.A. Dumesic, RuSn bimetallic catalysts for selective hydrogenation of levulinic acid to γ-valerolactone, Appl. Catal. B: Environ. 117-118 (2012) 321–329.

[16] M. Sudhakar, V.V. Kumar, G. Naresh, M.L. Kantam, S.K. Bhargava, A. Venugopal, Vapor phase hydrogenation of aqueous levulinic acid over hydroxyapatite supported metal (M = Pd, Pt, Ru, Cu, Ni) catalysts, Appl. Catal. B: Environ. 180 (2016) 113–120.

[17] Y. Zhang, C. Chen, W. Gong, J. Song, H. Zhang, Y. Zhang, G. Wang, H. Zhao, Self-assembled Pd/CeO₂ catalysts by a facile redox approach for high-efficiency hydrogenation of levulinic acid into gamma-valerolactone, Catal. Commun. 93 (2017) 10–14.

[18] M.L. Testa, L. Corbel-Demailly, V. La Parola, A.M. Venezia, C. Pinel, Effect of Au on Pd supported over HMS and Ti doped HMS as catalysts for the hydrogenation of levulinic acid to γ-valerolactone, Catal. Today 257 (2015) 291–296.

[19] K. Hengst, M. Schubert, H.W.P. Carvalho, C. Lu, W. Kleist, J.-D. Grunwaldt, Synthesis of γ-valerolactone by hydrogenation of levulinic acid over supported nickel catalysts, Appl. Catal. A: Gen. 502 (2015) 18–26.

[20] K. Shimizu, S. Kanno, K. Kon, Hydrogenation of levulinic acid to γ-valerolactone by Ni and MoOₓ co-loaded carbon catalysts, Green Chem. 16 (2014) 3899–3903.

[21] S. Gundekari, K. Srinivasan, In situ generated Ni(0)@boehmite from NiAl-LDH: An efficient catalyst for selective hydrogenation of biomass derived levulinic acid to γ-valerolactone, Catal. Commun. 102 (2017) 40–43.

[22] K. Jiang, D. Sheng, Z. Zhang, J. Fu, Z. Hou, X. Lu, Hydrogenation of levulinic acid to γ-valerolactone in dioxane over mixed MgO–Al₂O₃ supported Ni catalyst, Catal. Today 274 (2016) 55–59.

[23] V.V. Kumar, G. Naresh, M. Sudhakar, J. Tardio, S.K. Bhargava, A. Venugopal, Role of Brønsted and Lewis acid sites on Ni/TiO₂ catalyst for vapour phase hydrogenation of levulinic acid: Kinetic and mechanistic study, Appl. Catal. A: Gen. 505 (2015) 217–223.

[24] S. Song, S. Yao, J. Cao, L. Di, G. Wu, N. Guan, L. Li, Heterostructured Ni/NiO composite as a robust catalyst for thehydrogenation of levulinic acid toγ-valerolactone, Appl. Catal. B: Environ. 217 (2017) 115–124.

[25] A.M. Hengne, C.V. Rode, Cu–ZrO₂ nanocomposite catalyst for selective hydrogenation of levulinic acid and its ester to γ-valerolactone, Green Chem. 14 (2012) 1064.

[26] S.S.R. Gupta, M.L. Kantam, Selective hydrogenation of levulinic acid into γ-valerolactone over Cu/Ni hydrotalcite-derived catalyst, Catal. Today (2018) in press.

[27] B. Putrakumar, N. Nagaraju, V.P. Kumar, K.V.R. Chary, Hydrogenation of levulinic acid to γ-valerolactone over copper catalysts supported on γ-Al₂O₃, Catal. Today 250 (2015) 209–217.

[28] K. Yan, A. Chen, Selective hydrogenation of furfural and levulinic acid to biofuels on the ecofriendly Cu–Fe catalyst, Fuel 115 (2014) 101–108.

[29] P.P. Upare, M.G. Jeong, Y.K. Hwang, D.H. Kim, Y.D. Kim, D.W. Hwang, U.H. Lee, J.S. Chang, Nickel-promoted copper–silica nanocomposite catalysts for hydrogenation of levulinic acid to lactones using formic acid as a hydrogen feeder, Appl. Catal. A: Gen. 491 (2015) 127–135.

[30] Z. Li, M. Zuo, Y. Jiang, X. Tang, X. Zeng, Y. Sun, T. Lei, L. Lin, Stable and efficient CuCr catalyst for the solvent-free hydrogenation of biomass derived ethyl levulinate to γ-valerolactone as potential biofuel candidate, Fuel 175 (2016) 232–239.

[31] J. Zhou, L. Guo, X. Guo, J. Mao, S. Zhang, Selective hydrogenolysis of glycerol to propanediols on supported Cu-containing bimetallic catalysts, Green Chem. 12 (2010) 1835–1843.

[32] L.Y. Guo, J.X. Zhou, J.B. Mao, X.W. Guo, S.G. Zhang, Supported Cu catalysts for the selective hydrogenolysis of glycerol to propanediols, Appl. Catal. A: Gen. 367 (2009) 93–98.

[33] J. Zhou, J. Zhang, X. Guo, J. Mao, S. Zhang, Ag/Al$_2$O$_3$ for glycerol hydrogenolysis to 1,2-propanediol: activity, selectivity and deactivation, Green Chem. 14 (2012) 156–163.

[34] R. Morrish, A.J. Muscat, Nanoporous silver with controllable optical properties formed by chemical dealloying in supercritical CO$_2$, Chem. Mater. 21 (2009) 3865–3870.

[35] M.G. Méndezmedrano, E. Kowalska, A. Lehoux, A. Herissan, B. Ohtani, D. Bahena, V. Briois, C. Colbeaujustin, J.L. Rodríguezlópez, H. Remita, Surface modification of TiO$_2$ with Ag nanoparticles and CuO nanoclusters for application in photocatalysis, J. Phys. Chem. C 120 (2016) 5143–5154.

[36] M.K. Seery, R. George, P. Floris, S.C. Pillai, Silver doped titanium dioxide nanomaterials for enhanced visible light photocatalysis, J. Photochem. Photobiol. A: Chem. 189 (2007) 258–263.

[37] K.M. Kotesh, K. Bhavani, G. Naresh, B. Srinivas, A. Venugopal, Plasmonic resonance nature of Ag-Cu/TiO$_2$ photocatalyst under solar and artificial light: Synthesis, characterization and evaluation of H$_2$O splitting activity, Appl. Catal. B: Environ. 199 (2016) 282–291.

[38] X. Jiang, N. Koizumi, X.W. Guo, C.S. Song, Bimetallic Pd-Cu catalysts for selective CO$_2$ hydrogenation to methanol, Appl. Catal. B: Environ. 170 (2015) 173–185.

[39] J. Liu, F. Chen, Plasmon enhanced photoelectrochemical activity of Ag-Cu nanoparticles on TiO$_2$/Ti substrates, Int. J. Electrochem. Sci. 7 (2012) 9560–9572.

[40] R. Ferrando, J. Jellinek, R.L. Johnston, ChemInform abstract: Nanoalloys: From theory to applications of alloy clusters and nanoparticles, Chem Rev. 108 (2008) 845–910.

[41] S.H. Wei, A.A. Mbaye, L.G. Ferreira, A. Zunger, First-principles calculations of the phase diagrams of noble metals: Cu-Au, Cu-Ag, and Ag-Au, Phys. Rev. B 36 (1987) 4163–4185.

[42] A.M. Hilmen, D. Schanke, K.F. Hanssen, A. Holmen, Study of the effect of water on alumina supported cobalt Fischer–Tropsch catalysts, Appl. Catal. A: Gen 186 (1999) 169–188.

[43] N. Chandrasekharan, P.V. Kamat, Improving the photoelectrochemical performance of nanostructured TiO$_2$ films by adsorption of gold nanoparticles, J. Phys. Chem 104 (2000) 10851–10857.

[44] A. Takai, P.V. Kamat, Capture, store, and discharge shuttling photogenerated electrons across TiO$_2$-silver interface, ACS Nano. 5 (2011) 7369–7376.

[45] L. Liu, G. Wang, Y. Li, Y. Li, J.Z. Zhang, CdSe quantum dot-sensitized Au/TiO$_2$ hybrid mesoporous films and their enhanced photoelectrochemical performance, Nano Res. 4 (2011) 249–258.